

Synthesis of SrFe₁₂O₁₉ and Sr₇Fe₁₀O₂₂ systems for visible light photocatalytic studies

Rekha Dom^a, Pramod H. Borse^{a,*}, C. R. Cho^b, J. S. Lee^c, S. M. Yu^d, J. H. Yoon^d, T. E. Hong^d, E. D. Jeong^d and H. G. Kim^{d,*}

^aSolar H₂ PEC Lab, International Advanced Research Center for Powder Metallurgy and New Materials (ARC International), Balapur PO, Hyderabad, AP, 500-005, India

^bCollege of Nanoscience and Nanotechnology, Pusan National University, Busan 609-735, Korea

^cDepartment of Chemical Engineering, Pohang University of Science and Technology, Pohang 790-784, Korea

^dBusan Center, Korea Basic Science Institute, Busan 609-735, Korea

Solid state synthesis of two Sr-Fe-O systems *viz.* Sr₇Fe₁₀O₂₂ and SrFe₁₂O₁₉ was attempted and they were investigated for their photocatalytic properties. Although, both the systems exhibited good crystallinity and optical properties, only Sr₇Fe₁₀O₂₂ was found to be active for the photocatalytic decomposition of iso-propanol under visible light. It also yielded a significant quantum yield (~1.7%) for photo-reduction of water under visible light irradiation, much better than titanium oxy-nitride samples. The inactiveness of SrFe₁₂O₁₉ was due to its unsuitable band energetics. The Sr₇Fe₁₀O₂₂ acted more efficiently than TiO_{2-x}N_x due to its suitable band positions and high visible light photon absorptivity.

Key words: Strontium ferrite, Photocatalyst, Method, Visible light, Photocatalytic activity.

Introduction

In spite of the fact, that visible light is far more abundant and useful for an efficient photocatalysis under solar light; there has been a remarkable progress of UV-active photo catalysts during the last decade. Consequently, the development of visible light photocatalysts has become an important topic in photocatalysis research today. To date, several research groups have developed visible active photocatalysts of oxides, sulfides and oxynitrides such as PbBi₂Nb₂O₉, (Ga_{1-x}Zn_x)(N_{1-x}O_x), BaFe₂O₄, Bi₅Ti₃FeO₁₅, TaON, TiO_{2-x}N_x, TiO_{2-x}C_x, and Sm₂Ti₂O₅S₂, Fe-Cr co-doped TiO₂ *etc.* [1-10]. In search of highly efficient photocatalysts under visible light irradiation, we have recently discovered a novel single oxide PbBi₂Nb₂O₉ photocatalyst, and few of its proto-type designed oxides [11-14]. But, we still need highly efficient, small band gap (ca. 1.9~2.1 eV) photocatalysts, which will not only efficiently absorb the visible light photons from the solar spectrum but also are “ecofriendly”.

Ferrite systems are seen as one of the most important eco-friendly candidate photocatalysts [15-20]. The ferrite systems generally offer the advantage of yielding low band gap materials which are desirable for visible light active photo catalysts; additionally their abundance in nature cannot be overlooked. Strontium ferrites *viz.* Sr₇Fe₁₀O₂₂ and SrFe₁₂O₁₉ are such ferrite systems which

display interesting optical properties. In the present study we have identified these ferrites as possible visible active photo catalysts. These ferrites are known to exist in the form of orthorhombic (Sr₇Fe₁₀O₂₂) and hexagonal (SrFe₁₂O₁₉) crystal structures, and display low band gaps (~2 eV) desirable for a visible light photocatalyst. These systems can be formed under very high temperature conditions. We synthesized two systems, and carried out their photo catalytic characterization to confirm their candidacy for visible light active photo-catalysis. Accordingly we investigated the photocatalytic and the photoelectrochemical performance of these ferrites for photocurrent generation and CO₂ production from the photo-oxidation of iso-propyl alcohol (IPA), all under visible light irradiation ($\lambda \geq 420$ nm). The important implication of photocatalytic hydrogen formation of these ferrites was also studied from an energy generation perspective. Consequently, we systematically studied photocatalytic hydrogen generation under visible light photons over these photocatalysts. Sr₇Fe₁₀O₂₂ was found to be a much more active photocatalyst than the recently reported TiO_{2-x}N_x [5].

Experimental

Crystalline Sr₇Fe₁₀O₂₂ and SrFe₁₂O₁₉ photocatalysts were synthesized by a solid state reaction (SSR) method. Stoichiometric amounts of SrCO₃ (99.7%, Aldrich) and Fe₂O₃ (99%, Aldrich) powders were mixed and ground in methanol. The pelletized powders were calcined at 1000-1300 °C for 5 h in a static

*Corresponding author:

Tel : +82-51-974-6104

Fax: +82-51-974-6116

E-mail: phborse@arci.res.in ; hhgkim@kbsi.re.kr

furnace. On the other hand, for the purpose of comparison, $\text{TiO}_{2-x}\text{N}_x$ photocatalyst was also prepared by the hydrolytic synthesis method (HSM) [21]. Accordingly, an aqueous ammonium hydroxide solution (with an ammonia content of 28-30% (99.99%, Aldrich) was slowly added dropwise, to 20% titanium (III) chloride solution (TiCl_3 , Kanto, containing 0.01% iron as the major impurity) kept in an ice bath, for 30 minutes under aN_2 atmosphere, while continuously stirring the mixture. The suspension was stirred for 5 h to complete the reaction. After the completion of the reaction, the precipitate was filtered in air and washed several times with deionized water. The filtered powder was dried at 70 °C for 3-4 h in a convection oven. The sample obtained at this stage was an amorphous precipitate powder containing traces of ammonia and titanium. Further this sample was calcined at 400 °C for 2 h under air in an electric furnace to obtain the crystalline powder of $\text{TiO}_{2-x}\text{N}_x$.

The $\text{Sr}_7\text{Fe}_{10}\text{O}_{22}$ and $\text{SrFe}_{12}\text{O}_{19}$ samples were characterized using X-ray diffraction (XRD) using a Mac Science Co. M18XHF X-ray diffractometer. The XRD results were compared with the Joint Committee Powder Diffraction Standards (JCPDS) data for the phase identification of different samples. The optical properties *viz.* the band gap energy of the as-prepared powders was studied by a UV-Visible diffuse reflectance spectrometer (Shimadzu, UV 2401). The detailed structural characterization was carried out using high-resolution transmission electron microscopy (HR-TEM, Philips, CM 200). Further the photocatalytic characterization was carried out in the manner described below. About 200 ppm of gaseous IPA was injected into a 500-ml Pyrex reaction cell filled with air and 0.3 g of catalyst. The concentration of the reaction product

(CO_2) was determined by a gas chromatograph equipped with a thermal conductivity detector (CTR 1 packed column).

The photo-reduction reactions of water were carried out at room temperature in an upper-irradiation type Pyrex reaction vessel hooked up into a closed gas circulation system. Photocatalytic reduction was carried out by irradiating suspended powders using a Hg-arc lamp (500 W) equipped with a cutoff filter ($\lambda \geq 420$ nm). The H_2 evolution was examined in an aqueous methanol solution (distilled water 80 ml and CH_3OH 20 ml) by stirring 0.3 g of the catalyst loaded with 0.1 wt% Pt. Before photocatalytic reactions, all the catalysts were loaded with 0.1 wt% Pt using a conventional impregnation method using aqueous PtCl_2 . The concentration of the reaction product (H_2) was determined by a gas chromatograph equipped with a thermal conductivity detector (a molecular sieve 5-Å column and Ar carrier).

For photocurrent measurements, 25 mg of photocatalyst was suspended in distilled water (75 ml) containing acetate (0.1 M) and Fe^{3+} (0.1 mM) as an electron donor and as an acceptor, respectively, and the suspension pH was adjusted to 1.4 with HClO_4 . A platinum plate (1×1 cm², 0.125 mm thick, both sides exposed to the solution), a saturated calomel electrode (SCE), and a platinum gauze was immersed in the reactor as working (collector), reference, and counter electrodes, respectively. With continuous N_2 purging of the suspension, photocurrents were measured by applying a potential (+0.6 V vs. SCE) to the Pt electrode using a potentiostat (EG&G).

Results and Discussion

Figs. 1 & 2 show the XRD spectra of the corresponding

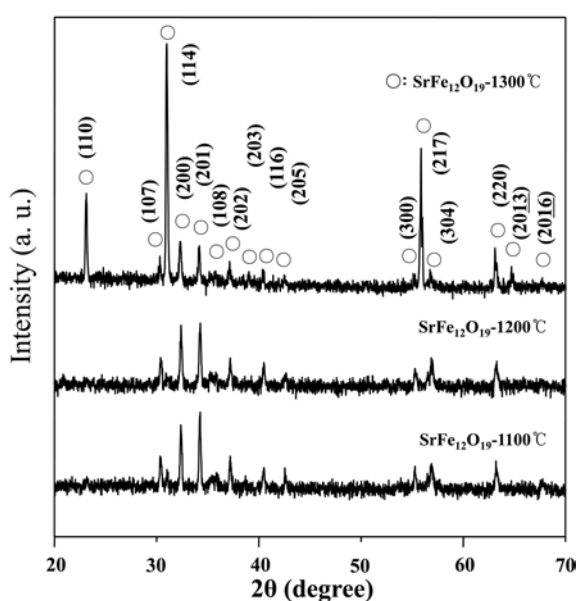


Fig. 1. XRD patterns of $\text{SrFe}_{12}\text{O}_{19}$ samples calcined at various temperatures in the range of 1100 °C-1300 °C.

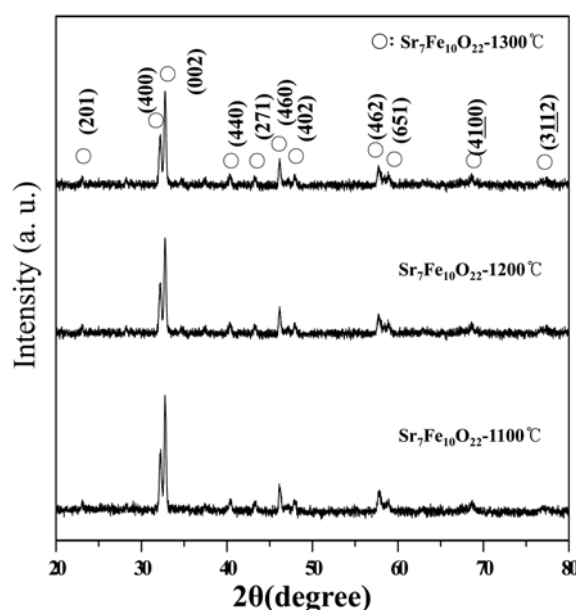
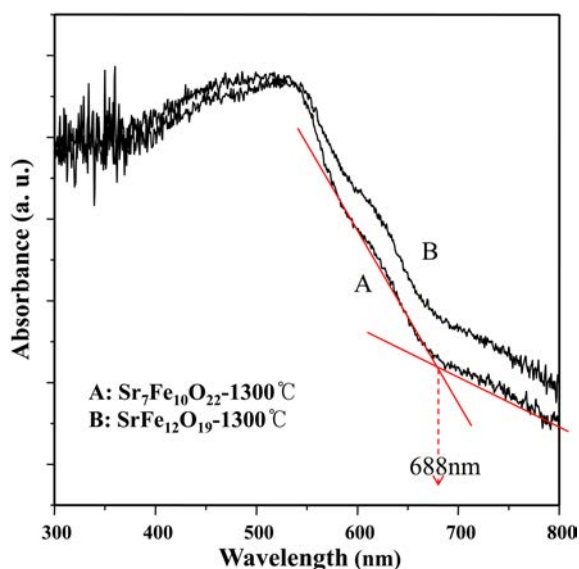


Fig. 2. XRD patterns of $\text{Sr}_7\text{Fe}_{10}\text{O}_{22}$ samples calcined at various temperatures in the range of 1100 °C-1300 °C.

Table 1. Energy band gap, calcination temperature and crystallite size of materials.

Material	Temperature (°C)	Crystallite size (nm)	Band gap (eV)
SrFe ₁₂ O ₁₉	1300	23.56	1.8
Sr ₇ Fe ₁₀ O ₂₂	1300	54.23	1.8
TiO _{2-x} N _x	400	13.3	2.73

**Fig. 3.** UV-Vis diffuse reflectance spectra of (A) Sr₇Fe₁₀O₂₂ and (B) SrFe₁₂O₁₉ calcined at 1300 °C for 5 h. The point of inflection indicates the band gap of the sample.

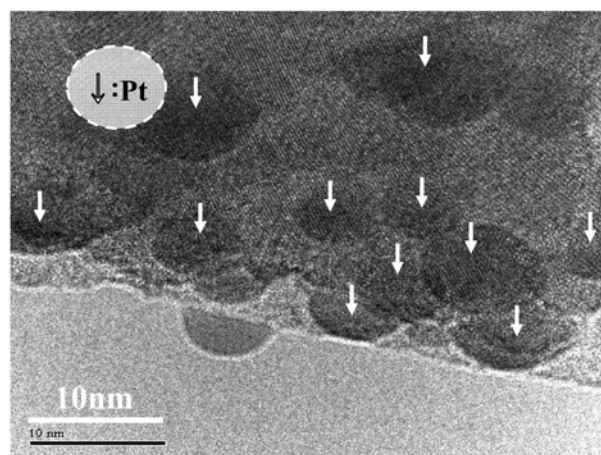
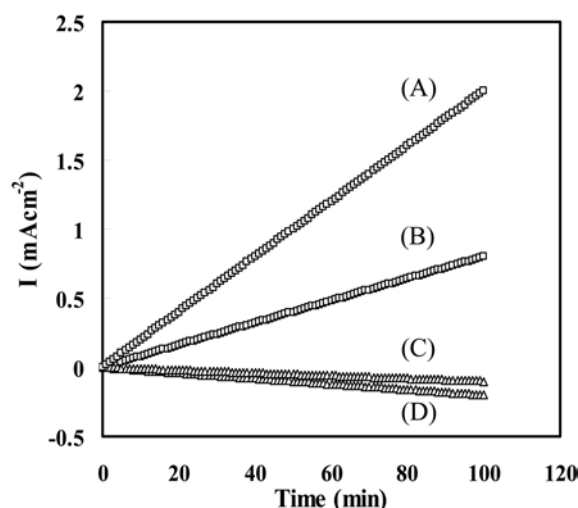
strontium ferrite samples, which were calcined in the temperature range of 1000-1300 °C in the SSR method. Fig. 1, clearly indicates the existence of a pure hexagonal SrFe₁₂O₁₉ phase (JCPDS Card No: 84-1531) for the case of the 1300 °C sample. Similarly, Fig. 2 does confirm the formation of the orthorhombic Sr₇Fe₁₀O₂₂ phase (JCPDS Card No: 26-0980) in the present study. The figures reveal that in either case, the crystallinity improved with an increase in the calcination temperature and finally acquires highly crystalline phases during the SSR syntheses.

The further observations reveal that the samples consist of nanocrystallites, as is evident from the Scherrer analysis for particle size determination. Table 1 shows the crystallite sizes of the respective systems, as estimated from the full width at half maxima (FWHM) of the main XRD peak in Figs. 1 and 2 using the Scherrer's equation [22]:

$$D = 0.9\lambda/\beta \cos\theta \quad (1)$$

where λ is the wavelength of the X-ray radiation ($\lambda = 0.154$ nm), β is the FWHM of the peak (in radians) corrected for instrumental broadening, θ is the Bragg angle, and D is the crystallite size (Å).

Fig. 3 shows the UV-visible diffuse reflectance

**Fig. 4.** HR-TEM image of a 1 wt% platinum-loaded Sr₇Fe₁₀O₂₂; 1 wt% of Pt was deposited on the base photocatalysts by a photo-deposition method under visible light ($\lambda \geq 420$ nm). Sr₇Fe₁₀O₂₂ was prepared by a solid state reaction method at 1300 °C.**Fig. 5.** The generated photocurrents under visible light ($\lambda \geq 420$ nm) irradiation for various material suspensions with acetate (electron donor) and Fe³⁺, (electron acceptor), respectively; (A) Sr₇Fe₁₀O₂₂; (B) TiO_{2-x}N_x; (C) SrFe₁₂O₁₉ and (D) TiO₂. Experimental conditions: photocatalysts = 0.025 g/75 ml; acetate = 0.1 M; Fe³⁺ = 0.1 mM; continuous N₂ purging; pH = 1.4; E_{app} = 0.6 V (vs SCE); Pt plate (10 × 10 × 0.125 mm), Pt-gauze as working and counter electrodes respectively.

spectra for SrFe₁₂O₁₉ and Sr₇Fe₁₀O₂₂, which were used for the estimation of band gaps (see Table 1). Both the systems showed a very good absorptivity for visible light photons and a small band gap indicating their semiconducting nature. This enabled us to utilize these systems for visible light photocatalysis.

To investigate the photocatalytic ability of the samples we tested them for visible light photo-degradation of IPA, a common model compound. In order to facilitate an efficient electron transfer, Pt was deposited on all the samples, prior to photocatalytic degradation. Fig. 4 displays the existence of the Pt particles over the base photocatalysts of the Sr-Fe-O system. The HR-TEM image (Fig. 4) of a 1 wt%

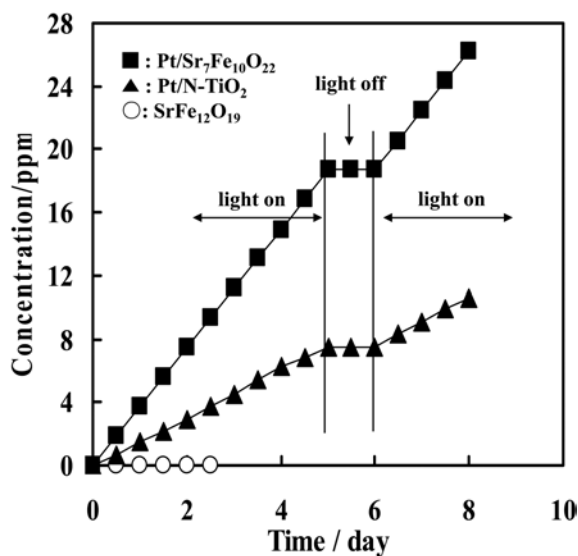


Fig. 6. Time course of CO₂ evolution from IPA decomposition over various materials under visible light irradiation ($\lambda \geq 420$ nm) in the presence of 1 g photocatalyst (a) Sr₇Fe₁₀O₂₂ (■), (b) TiO_{2-x}N_x (▲) and SrFe₁₂O₁₉ (○); IPA concentration, 200 ppm in air.

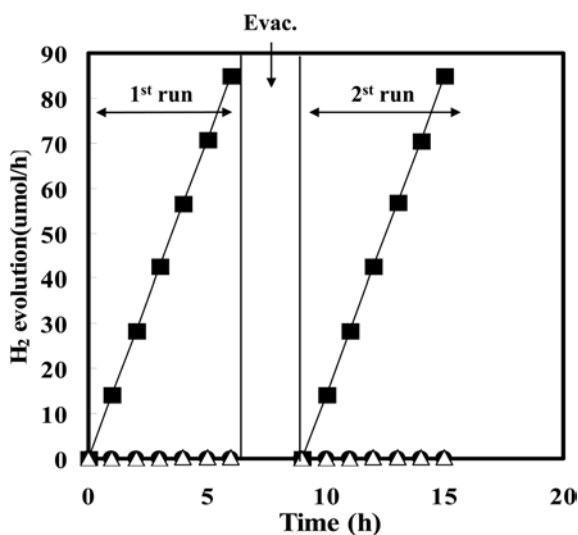


Fig. 7. Time course of H₂ gas evolution from Sr₇Fe₁₀O₂₂ (■), SrFe₁₂O₁₉ (●), and TiO_{2-x}N_x (△) under visible light irradiation, in an aqueous solution by stirring 0.1 g of catalyst loaded with Pt. The reaction system was evacuated every 5 h in order to remove gaseous products from the gas phase.

platinum-loaded Sr₇Fe₁₀O₂₂ displays the presence of well-dispersed > 5 nm platinum particles on the surface of Sr₇Fe₁₀O₂₂. This indicates that platinum is mostly deposited on the surface of the Sr₇Fe₁₀O₂₂ base catalyst.

Visible light active photocatalysts should generate photocurrents upon absorption of photons. To investigate the photocurrent generation, aqueous suspensions of the materials containing acetate (donor) and Fe³⁺ (acceptor) were illuminated with visible light ($\lambda \geq 420$ nm) photons. Fig. 5 shows the photocurrents generated over Sr₇Fe₁₀O₂₂, SrFe₁₂O₁₉, TiO_{2-x}N_x and TiO₂ samples. The Sr₇Fe₁₀O₂₂ sample generated a photocurrent approximately 3 times faster than TiO_{2-x}N_x sample, while the others did not

generate any photocurrent. The generation of a photocurrent means the critical initial step of photocatalytic reactions upon light irradiation. Thus, the photocurrent results can be directly correlated with the photocatalytic activity of the photocatalyst. The present study clearly indicates that Sr₇Fe₁₀O₂₂ is a much better visible-active photocatalyst than the others.

Following the above discussion, it is imperative that the Sr-Fe-O system can be utilized for the photocatalytic decomposition of a pollutant. Fig. 6 shows the rate of CO₂ evolution from the photo-degradation reaction over Sr₇Fe₁₀O₂₂, SrFe₁₂O₁₉ and TiO_{2-x}N_x samples. Sr₇Fe₁₀O₂₂ displayed efficient photocatalytic performance, whereas SrFe₁₂O₁₉ showed negligible CO₂ evolution. TiO_{2-x}N_x was considered as a standard visible light active photocatalyst for comparison. In the case of Sr₇Fe₁₀O₂₂, the concentration of CO₂ increased steadily with the irradiation time. The decomposition rate of IPA was significantly larger than the TiO_{2-x}N_x sample under visible light irradiation. The production of CO₂ gas stopped when light was turned OFF and restarted at the same rate when light was turned ON again. The photocatalytic activity of TiO_{2-x}N_x for IPA decomposition was less than that of Sr₇Fe₁₀O₂₂. Therefore, we investigated the superiority of the Sr₇Fe₁₀O₂₂, as analyzed in the following section.

We performed the photo-reduction reaction of water-methanol mixtures under visible light (≥ 420 nm). Fig. 7 shows the photocatalytic activity of different samples under the study indicating that Sr₇Fe₁₀O₂₂ yielded significant H₂ evolution in contrast to trace (TiO_{2-x}N_x) and no (SrFe₁₂O₁₉) evolution from the others. The hydrogen production over the Sr₇Fe₁₀O₂₂ sample increased steadily with the reaction time, following this the photoreaction system was evacuated for 5 h in order to remove gaseous products as seen from Fig. 7. Thus one can conclude that H₂ evolution over the photocatalysts occurred photo-catalytically. The photocatalytic quantum yield (QY) of the photocatalyst was calculated using the following equation [23, 24]:

$$QY = H_2 \text{ evolution rate} / 12.639 \times [(I_1 - I_3) - (I_1 - I_2)] \times A_1 / A_2 \times 100 \quad (2)$$

where I_1 is the blank light intensity, I_2 is the scattered light intensity, I_3 is the photocatalyst light intensity, A_1 is the lighted area of the photo reactor, A_2 is the area of the sensor face, and 12.639 is the mole number of photons with $\lambda \geq 420$ nm emitted from the lamp for 1 h. Estimation of QYs indicate that the Sr₇Fe₁₀O₂₂ sample shows a significant value of 1.77%. This is an important achievement with respect to the standard reference photocatalyst of the titanium oxynitride sample.

Further, fig. 8 shows the schematic of band energetics for the Sr₇Fe₁₀O₂₂, SrFe₁₂O₁₉ and TiO_{2-x}N_x systems as derived from the flat band potential measurements. Although the conduction/valence band edges of TiO₂

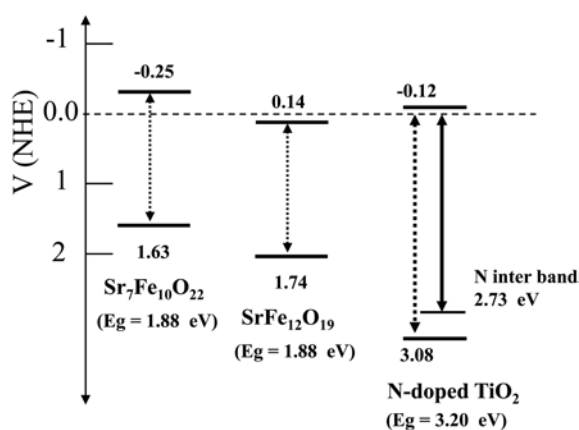


Fig. 8. A schematic band structures of $\text{Sr}_7\text{Fe}_{10}\text{O}_{22}$, $\text{SrFe}_{12}\text{O}_{19}$ and $\text{TiO}_{2-x}\text{N}_x$ as derived from flat band potential measurements. The estimated electrochemical potentials (vs. NHE) and the band positions at pH = 7 for different materials, displayed along with the respective calculated band gaps measurements.

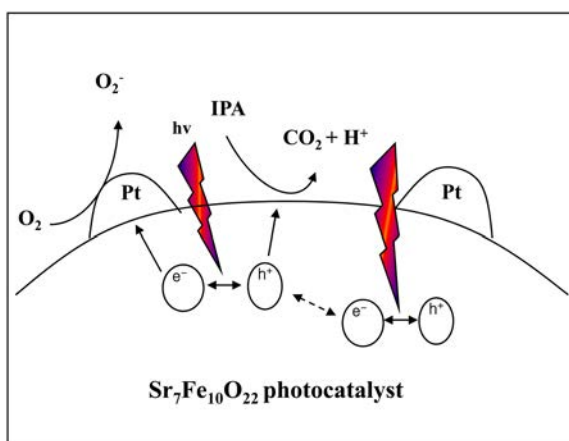


Fig. 9. Schematic diagram displaying the photocatalytic hydrogen production mechanism from methanol-water solution over $\text{Sr}_7\text{Fe}_{10}\text{O}_{22}$ base photocatalyst.

$\text{TiO}_{2-x}\text{N}_x$ are well suited for redox reactions, it is clear that $\text{Sr}_7\text{Fe}_{10}\text{O}_{22}$ offers the advantage of not only possessing well suited conduction/valence band positions, but also it has a smaller band gap. In the case of the $\text{SrFe}_{12}\text{O}_{19}$ system, the conduction band is not suited for photo-reduction of water, but only useful for photo-oxidation of water. Thus Fig. 9 clearly demonstrates the photocatalytic superiority of $\text{Sr}_7\text{Fe}_{10}\text{O}_{22}$ over others. Based on the aforesaid analysis we have also predicted the schematic of the working of the photocatalyst under visible light irradiation. Accordingly in order to photo-decompose IPA, the electron-holes generated in the $\text{Sr}_7\text{Fe}_{10}\text{O}_{22}$ are found to be effective during the reaction. Pt promotes the efficient transfer of electrons for the reduction reaction. Thus it is demonstrated that the $\text{Sr}_7\text{Fe}_{10}\text{O}_{22}$ photocatalyst is an efficient visible light photocatalyst than $\text{TiO}_{2-x}\text{N}_x$.

Conclusions

We have synthesized $\text{Sr}_7\text{Fe}_{10}\text{O}_{22}$ and $\text{SrFe}_{12}\text{O}_{19}$, two

Sr-Fe-O ternary oxide systems, by a simple solid state reaction method. Only $\text{Sr}_7\text{Fe}_{10}\text{O}_{22}$ was found to be active for the photocatalytic decomposition of iso-propanol and photo-reduction of water, under visible light. This is due to its semiconducting nature and appropriate band positions. The inactiveness of $\text{SrFe}_{12}\text{O}_{19}$ was due to its unsuitable physico-chemical properties. The $\text{Sr}_7\text{Fe}_{10}\text{O}_{22}$ was more efficient than $\text{TiO}_{2-x}\text{N}_x$ due to its suitable band positions and high visible light photon absorptivity.

Acknowledgement

The authors acknowledge the support of KBSI grant T30320, Hydrogen Energy R&D Center, Korea. One of the authors RD acknowledges the financial support of ARCI, DST lab, Hyderabad, India. The author (PB) also acknowledges the support of Director ARCI, Hyderabad.

References

- H.G. Kim, D.W. Hwang, J.S. Lee, *J. Am. Chem. Soc.* 126 (2004) 8912-8913.
- K. Maeda, T. Takata, M. Hara, N. Saito, Y. Inoue, H. Kobayashi, K. Domen, *J. Am. Chem. Soc.* 127 (2005) 8286-8287.
- P.H. Borse, C.R. Cho, K.T. Lim, Y.J. Lee, T.E. Hong, J.S. Bae, E.D. Jeong, H.J. Kim and H.G. Kim, *J. Korean Phys. Soc.* 58 (2011) 1672-1676.
- J.S. Jang, P.H. Borse, J.S. Lee, K.T. Lim, C.R. Cho, E.D. Jeong, M.G. Ha, M.S. Won, H.G. Kim, *J. Nanosci. Nanotech.* 10 (2010) 5008-5014.
- G. Hitoki, T. Takata, J. Kondo, M. Hara, H. Kobayashi, K. Domen, *Chem. Commun.* (2002) 1698-1699.
- R. Asahi, T. Ohwaki, K. Aoki, Y. Taga, *Science* 293 (2001) 269-271.
- SUM. Khan, M. Al-Shahry, W.B. Jr. Ingler, *Science* 297 (2002) 2243-2245.
- S. Sakthivel, H. Kisch, *Angew. Chem. Int. Ed.* 42 (2003) 4908-4911.
- E.D. Jeong, P.H. Borse, J.S. Jang, J.S. Lee, Ok-Sang Jung, H. Chang, J.S. Jin, M.S. Won and H.G. Kim, *J. Ceram. Proc. Res.* 12 (2011) 250-253.
- P.H. Borse, C.R. Cho, K.T. Lim, J.S. Bae, E.D. Jeong, T.E. Hong, H.J. Kim and H.G. Kim, *J. Ceram. Proc. Res.* 12 (2011) 592-598.
- J.S. Jang, H.G. Kim, P.H. Borse, J.S. Lee, *Inter. J. Hydrogen Energy* 32 (2007) 4786-4791.
- J.S. Jang, H.G. Kim, U.A. Joshi, J.W. Jang, J.S. Lee, *Inter. J. Hydrogen Energy* 33 (2008) 5975-5980.
- H.G. Kim, P.H. Borse, W. Choi, J.S. Lee, *Angew. Chem. Int. Ed.* 44 (2005) 4585-4589.
- H.G. Kim, E.D. Jeong, P.H. Borse, S. Jeon, K. Yong, J.S. Lee, Li W, S.H. Oh, *Appl. Phys. Lett.* 89 (2006) 0641031-3.
- H.G. Kim, P.H. Borse, J.S. Jang, O. Jung, Y.J. Suh, J.S. Lee, *Chem. Comm.* (2009) 5889-5891.
- E.D. Jeong, P.H. Borse, J.S. Jang, J.S. Lee, C.R. Cho, J.S. Bae, S. Park, O.S. Jung, S.M. Ryu, M.S. Won, H.G. Kim, *J. Nanosci. Nanotech.* 9 (2009) 3568-3573.
- X. Wang, Y. Lin, X. Ding, J. Jiang, *J. Alloys Compd.* (2011) 6585-6588.
- C-H Chen, Y-H Liang, W-D Zhang, *J. Alloys Compd.* 501

- (2010) 168-172.
19. H. Yang, J. Yan, Z. Lu, X. Cheng and Y. Tang, *J. Alloys Compd.* 476 (2009) 715-719.
20. Z. Wang, S. Zhu, S. Zhao, H. Hu. *J. Alloys Compd.* 509 (2011) 6893-6898.
21. J.S. Jang, H.G. Kim, S.M. Ji, S.W. Bae, J.H. Jung, B.H. Shon, J.S. Lee, *J Solid State Chem.* 179 (2006) 1067-1075.
22. B.D. Cullity, *Elements of X-ray Diffraction*, 2nd Edition, (Addison-Wesley Publishing Company, Inc., Reading, MA 1978).
23. S.W. Bae, P.H. Borse, S.J. Hong, J.S. Jang, J.S. Lee, E.D. Jeong, T.E. Hong, J.H. Yoon, J.S. Jin, H.G. Kim. *J. Korean Phys. Soc.* 51 (2007) S22-S26.
24. S.J. Hong, P.H. Borse, S.M. Ji, J.S. Jang, J.S. Lee, E.D. Jeong, H.G. Kim, H.K. Park, *J. Korean Phys. Soc.* 51 (2007) S27-S31.